ACS APPLIED MATERIALS & INTERFACES

Research Article

www.acsami.org

Osteoinductive Fibrous Scaffolds of Biopolymer/Mesoporous Bioactive Glass Nanocarriers with Excellent Bioactivity and Long-Term Delivery of Osteogenic Drug

Ahmed El-Fiqi,[†,‡,⊥] Joong-Hyun Kim,[†,‡] and Hae-Won Kim*[,†,‡,§]

[†]Institute of Tissue Regeneration Engineering (ITREN), Dankook University, Cheonan 330-714, South Korea

[‡]Department of Nanobiomedical Science and BK21 PLUS NBM Global Research Center for Regenerative Medicine, Dankook University, Cheonan 330-714, South Korea

[⊥]Glass Research Department, National Research Center, Cairo, Egypt

[§]Department of Biomaterials Science, School of Dentistry, Dankook University, Cheonan 330-714, South Korea

ABSTRACT: Designing scaffolds with bioactive composition and long-term drug delivery capacity is a promising method to improve the therapeutic efficacy in bone regeneration. Herein, electrospun fibrous scaffolds of polycaprolactone-gelatin incorporating mesoporous bioactive glass nanoparticles (mBGn) were proposed to be excellent matrix platforms for bone tissue engineering. In particular, the mBGn were loaded with osteogenic drug Dexamethasone (DEX) to elicit additional therapeutic potential. The mBGn-added fiber scaffolds demonstrated excellent properties, including improved mechanical tensile strength, elasticity, and hydrophilicity compared to pure biopolymer matrix. The scaffolds could release substantial amounts of calcium and silicate ions. The loading of DEX onto mBGn was as high as 63%, that is, 0.63 mg DEX loaded per 1 mg of mBGn, demonstrating an effective nanodepot role of the mBGn. The release of DEX from the mBGn-added fiber scaffolds was highly sustainable, profiling an almost linear release kinetics up to the test period of 28 days, after a rapid initial release of ~30% within 24 h. The proliferation and osteogenic differentiation of stem cells derived from periodontal ligament were significantly improved by the mBGn incorporation and synergistically stimulated with DEX loading, as confirmed by both direct and indirect cultures. The effects on bone regeneration in vivo, as analyzed by microcomputed tomography and histological stains in a rat calvarium model over 6 weeks, were substantial with the mBGn incorporation and even better with DEX loading, evidencing the osteogenic effects of the drug-eluting nanocomposite fiber scaffolds in bone formation. The current scaffolds with bone-bioactive composition and drug delivery capacity may be potentially useful for bone regeneration as novel osteogenic matrices.

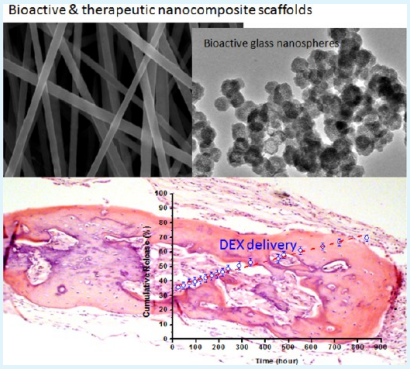

KEYWORDS: *therapeutic scaffolds, drug delivery, bone regeneration, mesoporous nanoparticles, bioactive glass, dexamethasone*

1. INTRODUCTION

Designing scaffolds with bioactivity and drug delivery capacity is a promising approach to regulate cellular behaviors and to improve the bone regeneration processes.[1,2] The bioactive surface of scaffolds can stimulate initial cellular events, including adhesion and spreading. Furthermore, the anchored cells can multiply and differentiate properly in response to the therapeutic signals provided by the scaffolds.[3]

Targeting bone tissue, the nanocomposite approach of combining organic and inorganic compositions is considered to be promising; while the organic matrix provides resilience and shape-formability, the inorganic nanocomponent improves bioactivity and mechanical strength.[4,5] Among the scaffold forms, the fibrous morphology, with its tissue-mimicking architecture, has been widely used to culture stem cells and to repair damaged tissues including bone.[6−8] Osteoprogenitor or stem cells have been shown to readily recognize the fibrous architecture, develop their shape along the fibers, and consequently differentiate into an osteogenic lineage under proper biochemical cues.[6−8]

Some of our recent works have developed various nanocomposite scaffolds with fibrous forms for bone regeneration.[9−11] Depending on the biopolymer composition, whether it is in synthetic or natural form, the incorporation methods of inorganic nanocomponents need to be considered, which include in situ precipitation, surfactant-mediated inclusion, or direct homogenization.[12,13] Among the nanocomponents developed, including hydroxyapatite nanoparticles, bioactive glass nanofibers, and calcium carbonate nanoparticles,[14−17] the mesoporous form is highly effective for loading therapeutic molecules and their subsequent delivery.[18−20] In fact, mesoporous silica nanoparticles have been the most-widely studied nanomaterial form for drug delivery due to the highly

Received: October 5, 2014
Accepted: December 22, 2014
Published: December 22, 2014

DOI: 10.1021/am5077759
ACS Appl. Mater. Interfaces 2015, 7, 1140−1152

mesoporous structure.[21−23] However, mesoporous silica nanoparticles have low capacity for bone-like apatite formation and bone regeneration. To improve the bone regenerative ability, we recently developed mesoporous bioactive glass nanospheres (mBGn) that are also highly mesoporous.[24] Due to their surface activity related with the release of ions (calcium and silicon), the mBGn have been shown to accelerate acellular mineralization and to stimulate cell responses when used at proper doses.[25,26] Furthermore, the mBGn were effective in loading a series of therapeutic molecules, including small antibiotic drugs, proteins and genetic molecules, demonstrating their usefulness for nanodelivery systems.[24]

To this end, we aim to make full use of the mBGn multifaceted potential, that is, drug loading/delivering capacity and bone-bioactivity. We therefore incorporated the drug-loaded mBGn within the biopolymer fiber matrix to produce therapeutic nanocomposite scaffolds. Dexamethasone (DEX), an osteogenic drug, was chosen for the model drug to stimulate osteogenesis of stem cells and bone formation. The design of the bioactive nanocomposite fiber scaffolds that have the osteogenic capacity is schematically illustrated in Figure 1a. The physicochemical and mechanical properties of the mBGn-added fibrous scaffolds were briefly assessed, and the in vitro and in vivo osteogenic effects of the DEX-loaded scaffolds were studied in-depth for potential use in bone regeneration.

2. MATERIALS AND METHODS

2.1. Preparation of Nanocarriers and Nanocomposite Fiber Scaffolds. Analytical-grade materials were used for the nanocarriers and scaffolds preparation. Tetraethyl orthosilicate (TEOS,$C_8H_{20}O_4Si$, 98%), calcium nitrate tetrahydrate ($Ca(NO_3)_2{\cdot}4H_2O$, 99%), poly(ethylene glycol), (PEG, $(C_2H_4)_nH_2O$, M_n = 10000), ammonium hydroxide (NH_4OH, 28.0% NH_3 in water, ≥ 99.99% metal basis), methanol anhydrous (CH_3OH, 99.8%), gelatin (Gel, type B from bovine skin), 3-aminopropyl triethoxysilane (APTES, $C_9H_{23}NO_3Si$, ≥ 98%), toluene anhydrous (C_7H_8, 99.8%), poly(ε-caprolactone) (PCL, M_n = 70 000−90 000), 2,2,2-trifluoroethanol (TFE,CF_3CH_2OH, ≥ 99%), tris(hydroxymethyl aminomethane) (Tris-buffer), 1N hydrochloric acid (1N HCl) and phosphate buffered saline (PBS) tablets were all purchased from Sigma-Aldrich and were used as-received without any further purification. Dexamethasone 21-phosphate disodium salt (DEX, $C_{22}H_{28}FNa_2O_8P$ ≥ 98%), used as the model drug, was purchased from Sigma-Aldrich. Ultrapure deionized water (18.2 MΩ·cm) was obtained from Millipore Direct-Q system.

The mBGn, with a composition of 75%SiO_2/25%CaO (mol %), were prepared using an ultrasound assisted base-catalyzed sol−gel method, as described elsewhere.[9] In a typical synthesis, 5 g of PEG was dissolved in 120 mL of absolute methanol with pH adjusted to 12.5 by adding NH_4OH. Next, 0.299 g Ca $(NO_3)_2{\cdot}4H_2O$ was added and dissolved with vigorous stirring. In a separate vial, 0.793 g of TEOS was diluted with 30 mL of absolute methanol and added dropwise to the pH-adjusted solution with ultrasound for 20 min. The white precipitate obtained after 24 h of stirring was separated and washed using water/ethanol in three centrifugation/redispersion cycles at 5000 rpm for 5 min and then dried at 70 °C overnight. To remove the PEG template, the dried powder was calcined at 600 °C for 5 h. The calcined nanopowders were stored under vacuum for further use. The nanopowders were then surface functionalized with $-NH_2$ groups. Briefly, 100 mg of nanoparticles was dispersed in 50 mL of anhydrous toluene and refluxed, under stirring, with 1 mL of APTES at 80 °C for 12 h. The NH_2-functionalized nanoparticles were then collected by centrifugation and washed with toluene before final drying at 80 °C under vacuum for 24 h.

The fibrous scaffolds were prepared using the electrospinning technique. For the biopolymer fiber, 10 wt % gelatin and 10 wt % PCL solutions in TFE were separately prepared under magnetic stirring at 40 °C, and then both solutions were mixed at 1:1 weight ratio and stirred to homogenize. For the mBGn-added fibers, 2.5, 5, and 10 wt % mBGn (with respect to biopolymer weight) were first dispersed separately in both 10 wt % gelatin and 10 wt % PCL solution, and then the two mixtures were homogenized. The prepared composite polymer solutions were then electrospun under the following conditions: injection rate, 1 mL/h; voltage, 10.5 V; distance,14.5 cm. Finally, the prepared electrospun fibrous sheet was allowed to completely evaporate any residual TFE solvent and stored under vacuum for further use.

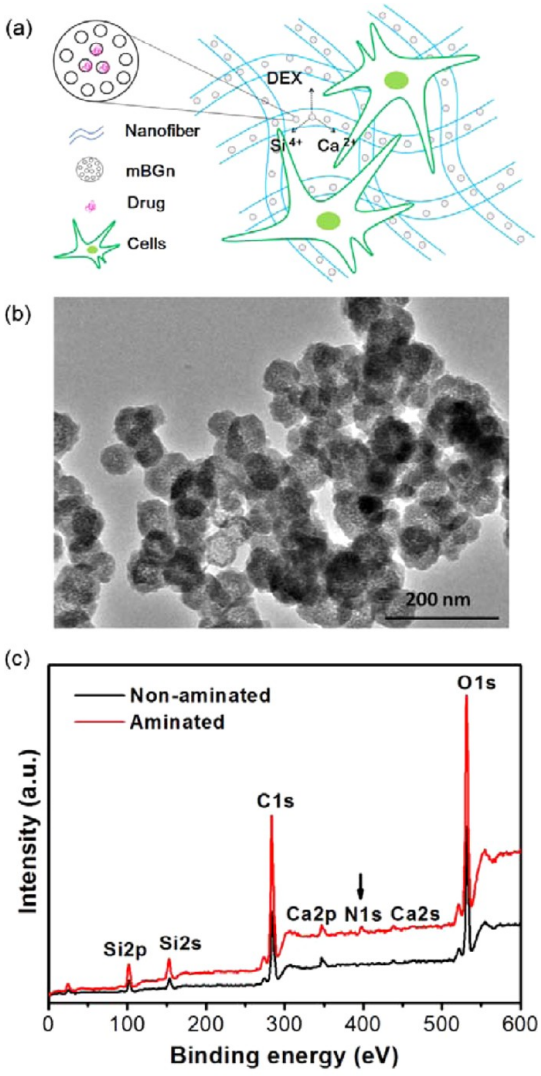

Figure 1. (a) Schematic diagram showing the therapeutic fiber scaffolds incorporating DEX-loaded mBGn, where the drug releasing effect and bioactivity of mBGn can be synergized to regulate osteogenic responses. (b) TEM image of aminated-mBGn and (c) XPS analysis showing the additional nitrogen peak in the aminated mBGn.

2.2. Characterizations. The surface composition of the samples was examined before and after surface amination by X-ray photoelectron spectroscopy (XPS; ESCA 2000, V.G. Microtech, United Kindgom) with a monochromatic Al Kα source (1486.6 eV). The surface ζ-potential of samples was measured using a Laser Doppler electrophoresis (LDE) instrument (Zetasizer Nano ZS, Malvern Instruments, United Kindgom). The mesoporosity of the nanoparticles was obtained by N_2 adsorption−desorption measurement (Quadrasorb SI, Quantachrom Instruments, Ltd., Boynton Beach, FL). The specific surface area was calculated according to the Brunauer−Emmett−Teller (BET) method, and the pore size distribution was

DOI: 10.1021/am5077759
ACS Appl. Mater. Interfaces 2015, 7, 1140−1152

determined based on the nonlocal density functional theory (NLDFT) method.

The morphology of the prepared samples was observed by scanning electron microscopy (SEM, JSM-6510, JEOL, Japan), and high-resolution transmission electron microscopy (HR-TEM, JEM-3010, JEOL, Japan) equipped with energy dispersive X-ray spectrometry (EDX, Oxford Instruments). The phase of the samples was analyzed by X-ray diffraction (XRD, Rigaku, Ultima IV, Japan) at a scanning speed of 2°/min. The chemical bond structure of samples was examined by attenuated total reflectance Fourier transform infrared (ATR-FTIR; Varian 640-IR, Australia) with a resolution of 4 cm^{-1}. The thermal behavior of the samples was observed by thermogravimetric analysis (TGA; TGA N-1500, Scinco, Ltd., South Korea) in nitrogen gas at a heating rate of 10 °C/min.

Surface hydrophilicity of the fiber scaffolds was assessed with water contact angle measurement using a benchtop Phoenix contact angle measurement system (PHX300, SEO, South Korea). One drop of deionized water (2 μL) was automatically dropped onto the sample surface. Images of the water droplets were recorded within 15 s using a video camera system (CCD camera) and the surface contact angles were calculated using Image XP software.

The in vitro degradability of the scaffolds was tested in phosphate buffer saline (PBS, pH = 7.4) at 37 °C. Samples were immersed in 10 mL of PBS for different time points up to 28 days, and PBS was refreshed every 3 days. The weight change during the test was recorded.

The in vitro apatite forming ability of the scaffolds was tested in simulated body fluid (SBF) at 37 °C. The SBF was prepared by dissolving NaCl (142.0 mM), $NaHCO_3$ (4.2 mM), KCl (5.0 mM), $K_2HPO_4{\cdot}3H_2O$ (1.0 mM), $MgCl_2{\cdot}6H_2O$ (1.5 mM), $CaCl_2$ (2.5 mM), and Na_2SO_4 (0.5 mM) into deionized water buffered to pH 7.4 with Tris-HCl at 37 °C. Each scaffold sample was immersed in 10 mL of SBF for up to 28 days, and SBF was refreshed daily. The surface of samples were examined by SEM, and the phase and chemical bond structure were analyzed by XRD and FT-IR, respectively.

The release of calcium and silicon ions from the samples was measured. Twenty mg of the nanoparticles or 200 mg of fiber scaffold samples were immersed in 10 mL deionized water, buffered to pH 7.4 with Tris-HCl, at 37 °C for up to 28 days. At predetermined time points, samples were collected for characterization with inductively coupled plasma atomic emission spectrometry (ICP-AES; OPTIMA 4300 DV, PerkinElmer, Waltham, MA).

The tensile mechanical properties of the scaffolds were determined using a tabletop uniaxial testing machine (Instron 5966, Norwood, MA) using a 500 N load cell with a cross-head speed of 10 mm/min. Samples were prepared with dimensions of 60 × 10 × 0.5 mm (thickness) and a gauge length of 40 mm. The stress−strain curves were recorded, and the elastic modulus, tensile strength, and elongation percentage were determined based on the curves. Five replicate measurements were carried out and then averaged.

2.3. DEX Loading and Release Tests. DEX is a form of phosphate disodium salt (negatively charged); therefore, we used aminated mBGn for the drug loading study. The loading capacity of DEX onto the aminated mBGn was investigated by dispersing the nanospheres at a concentration of 10 mg/mL in distilled water containing different concentrations of DEX (5, 10, 15, 20, 25, and 30 mg/mL). The amounts of DEX loaded were determined using UV−vis spectrometer (Libra S22, Biochrom, United Kingdom). A series of standard DEX solutions (0 and 100 μg/mL) were prepared for the calibration curve. A loading isotherm of DEX was obtained from the DEX adsorbed amounts according to the following mass balance equation: $q_e = (C_0 - C_e) \times (V/W)$, where q_e is the amount of DEX (in mg) adsorbed per mg mBGn, C_0 and C_e are the initial and equilibrium concentrations of DEX (mg/mL), respectively, V is the volume of solution (ml), and W is the weight of the mBGn sample used (mg).

The in vitro release of DEX from the bare mBGn was carried out in DW, and the release amount was quantified by UV measurement at 242 nm using the DEX calibration curve. Ten milligrams (10 mg) of mBGn loaded with 0.286 mg mg^{-1} (28.6% DEX) was dispersed in 50 mL DW and incubated at 37 °C for different time periods. At predetermined time points, 1 mL was withdrawn from the release medium for the DEX analysis. The DEX release from the fiber scaffold samples was then carried out. For this, the DEX-loaded mBGn (0.286 mg DEX per mg of mBGn) were incorporated in the polymer matrix at 2.5%. The 2.5% content of mBGn was considered to be high enough to show the DEX release profile. For the comparison group, free DEX was loaded within the fiber scaffold directly by dispersing DEX drug at the same quantity as that used for the nanocomposite fiber. The DEX-loaded scaffolds were completely dried and kept under vacuum for further release study.

The DEX release from the scaffolds was quantified by high performance liquid chromatography (HPLC). Fifty milligrams (50 mg) of each fiber scaffold was immersed in 10 mL DW and incubated at 37 °C. At predetermined time points, 1 mL of the release medium was withdrawn for DEX analysis, and the medium was refreshed with 1 mL of fresh DW. Collected samples were filtered with disposable syringe filters (0.20 μm, Avantec, Toyo Roshi Kaisha, Ltd., Japan) before analysis. The analyses were performed using HPLC instrument (ACME 9000 system, Younglin Instrument, Ltd., South Korea). The flow rate was adjusted to 1 mL/min, the column temperature was maintained at 37 °C, and UV detection was performed at 254 nm. The chromatographic separation was carried out on the Varian C18 column (150 × 4.6 mm, 5 μm) (VR-150) using a mixture of water/acetonitrile (40:60 v/v) as the mobile phase. DEX was detected at an average retention time of 1.18 min. A set of standard solutions of DEX in the concentration range of 10−100 μg/mL were prepared to obtain a linear calibration curve obeying the equation, $A = 28.686C - 27.668$ ($R^2 = 0.9988$, $n = 3$). A is the absorbance, and C (μg/mL) is the concentration.

2.4. In Vitro Cell Responses. Rat periodontal ligament stem cells (PDLSCs) were isolated from a 5-week-old male Sprague−Dawley (SD) rat. Briefly, four SD rat incisors were extracted, and the ligament tissues were scraped. After being washed, tissues were digested with 0.05% collagenase type I solution for 1 h at 37 °C. After 24 h of culture in normal medium (α-modified minimal essential medium with 10% fetal bovine serum and 100 U/ml penicillin and 100 mg/mL streptomycin), cells were collected by trypsinization (0.05% trypsin), resuspended and cultured for an additional 4 days until they reached near confluence. Cells were subcultured with refreshing medium every 2−3 days, and the cells at 3−4 passages were used for further experiments.

Three different scaffold groups were tested; biopolymer scaffold, 2.5%mBGn-added scaffold and 2.5%mBGn+DEX added scaffold. Prior to cell tests, samples with dimensions of 15 × 15 mm were prepared and sterilized with ethylene oxide gas. Two different culture designs were used to enable either "direct" or "indirect" interaction between cells and scaffolds. For the direct interaction, cells were directly plated onto the scaffold samples. A 100 μL aliquot of 5×10^4 PDLSCs was seeded onto each scaffold sample in each well of 24-well plates, which were then left in an incubator for 2 h. After this, the cell-seeded samples were transferred to another culture well for longer cultures. For the indirect test, 5×10^4 PDLSCs were plated onto each well of 24-well plates. After 2 h of cell adhesion, the scaffold sample was placed onto a Transwell insert, which was placed on top of the culture well, to enable only medium interactions between the cells and scaffold sample. After 24 h, the cell culture medium was replaced with the osteogenic medium free of dexamethasone (containing ascorbic acid and beta-glycerophysphate in addition to normal medium ingredients), after which the culture medium was refreshed every other day.

After the cells were cultured for predetermined time periods, the cells were trypsinized from the scaffold sample (direct test) or from the culture well (indirect test). Quantification of the cell proliferation was assessed by double-stranded DNA (dsDNA) fluorescence kit (PicoGreen quantitation assay kit, Molecular Probe). Briefly, the cultured cells were lysated, followed by three freezing/thawing cycles and the resultant supernatants were collected. Aliquots (50 μL) of the cell lysates were added in a 96-well assay plate and a 50 μL volume of a PicoGreen (Quant-iT PicoGreen assay kit; Invitrogen) was added to each well, and incubated for 5 min in the dark. The cell proliferation level was recorded by the fluorescence absorbance.

DOI: 10.1021/am5077759
ACS Appl. Mater. Interfaces 2015, 7, 1140−1152

For observation of the cell morphology, the cultured cells were washed and subsequently fixed with 4% paraformaldehyde, followed by a treatment with 0.2% Triton X-100. One percent (1%) bovine serum albumin solution (w/v) was treated for 30 min. Subsequently, Alexa Fluor 488-conjugated phalloidin and ProLong Gold antifade reagent with 4′,6-diamidino-2-phenylindole DAPI were used to stain F-actins and nuclei, and the cells were visualized via fluorescence microscope (IX71, Olympus, Tokyo, Japan).

To check the osteogenic differentiation of cells, we determined the enzymatic activity of alkaline phosphatase (ALP). After culture, the cell lysates were obtained after three freeze−thaw cycles (freezing at −80 °C for 20 min immediately followed by thawing at 37 °C for 10 min) and followed by addition of cell lysis buffer (0.2% Triton X-100). The cell lysate samples (50 μL) were added to 50 μL of working reagent containing equal parts (1:1:1) of 1.5 M 2-amino-2 methyl-1-propanol, 20 mM p-nitrophenol phosphate, and 1 mM magnesium chloride, and the samples were then incubated for 1 h at 37 °C. The reaction was stopped with the addition of 100 μL of 1 N NaOH on ice, and the absorbance was determined at 405 nm using microplate-reader (iMark, Bio-Rad, Hercules, CA). The ALP specific activity was calculated by normalizing to dsDNA produced from each sample. Each test was performed on three replicate samples (n = 3).

2.5. In Vivo Animal Studies. First, for the tissue compatibility study, the fiber scaffolds were implanted in rat subcutaneous tissue. Two representative groups of the fibrous scaffolds (2.5%mBGn with and without DEX) were prepared, and then sterilized with ethylene oxide gas before surgical operation. All experimental procedures for animal care and use were reviewed and approved in accordance to guidelines established by Dankook University Institutional Animal Care and Use Committee. Each rat (12 weeks old, male, Sprague−Dawley) received an intramuscular injection with ketamine at 80 mg/kg body weight and xylazine at 10 mg/kg body weight. A 2 cm skin incision was made, and four small subcutaneous pouches were created to place the scaffold specimen. The incision was sutured with monofilament suture (Prolene). The animals were sacrificed at 2 weeks postimplantation. Tissue samples were harvested and then immersed in 10% neutralized buffered formalin for 24 h. Samples were then dehydrated in graded ethanol series, paraffinized, bisected, and embedded in paraffin. Histological samples were prepared with 5 μm thickness using a rotary microtome (Leica RM2245, leicabiosystems, Germany) and were then stained with hematoxylin and eosin (H&E) or Masson's trichrome (MT).

Next, the in vivo bone-forming ability of the fiber scaffolds was examined in a rat calvarium defect model, as previously described.[26] A linear sagittal midline skin incision was made over the calvarium, and a full-thickness flap of the skin and periosteum was elevated. Two critical-sized full-thickness bone defects (5 mm diameter) were created at the center of each parietal bone in the calvarium using a trephine bur. Each cranial defect was randomly filled with 0%, 2.5%mBGn or 2.5%mBGn+DEX scaffold group. A total of nine rats were used for the implantation of the three sample groups (three rats for each group).

Six weeks after the operation, the animals were sacrificed, and calvaria specimens were harvested and fixed in 10% buffered neutralized formalin for 24 h. Prior to histological analysis, the calvaria specimens were scanned by in vivo X-ray microcomputed tomography (μCT). Following fixation, 3D images were taken using μCT scanner (SkyScan 1176; Skyscan, Aartselaar, Belgium) to analyze the new bone formation. The collected 3D scans were reconstructed and analyzed using CTAn (Skyscan). A cylindrical region of interest (ROI) was positioned over the center of the single defect, fully enclosing the new bone within the defect site. The percentages of new bone volume (%) and bone surface density (1/mm) were measured.

After μCT imaging and analysis, the harvested samples were prepared for histological analysis. The fixed specimens were decalcified with RapidCal solution (BBC Chemical Co., Stanwood), dehydrated through a series of ethanol solutions, and subsequently bisected and embedded in paraffin. Then, 5 μm thick sections were serially obtained from the central region of the circular defects and were defined as representative samples. The histological samples were stained with hematoxylin and eosin (H&E) stains and were finally visualized under optical microscope.

2.6. Statistical Analysis. The data are expressed as mean ± standard deviation, and statistical analysis was carried out by using one-way analysis of variance (ANOVA) followed by Fisher posthoc test. Statistical significance was considered at $p < 0.05$.

3. RESULTS AND DISCUSSION

3.1. mBGn Nanocarriers Used to Load Drug and to Provide Bone-Bioactivity. The mBGn, used as the bioactive nanocomponents in polymer matrices and as effective drug loading nanocarriers, were first developed using the sono-reacted sol−gel method under alkaline conditions. The surface of mBGn was further aminated to load the negatively charged DEX drug and to improve the DEX loading efficiency. The morphology and chemical composition of the nanocarriers were examined. The TEM image (Figure 1b) showed well-developed nanospheres with highly mesoporous structures and an average size of 62.7 nm ±12.3 nm (n = 350). A TEM-EDS analysis of the mBGn composition resulted in an atomic ratio of Si/Ca = 74/26, which closely match the Si/Ca ratio of the initially designed composition (Si/Ca = 75/25). The XPS wide canning of the nanocarriers revealed characteristic peaks of Si (2p, 104 eV; 2s, 155 eV), Ca (2p, 347 eV; 2s, 439 eV), O (1s, 530 eV) and C (1s, 285 eV). An additional peak at 400 eV, attributed to N 1s, was identified on the aminated nanocarrier, indicating the presence of surface amino groups (Figure 1c). The ζ−potential values were around −15.5 mV for non-aminated and +23.3 mV for aminated samples measured at pH 7.4, indicating the effect of amination on the surface charge. Furthermore, the pore properties of the aminated mBGn measured by the N_2 adsorption/desorption method demonstrated a high level of mesoporosity, including surface area (41.5 m^2/g), pore volume (0.08 cm^3/g), and mesopore size (3.51 nm), as summarized in Table 1. Based on these results, the mBGn are considered to provide effective mesopore space for the small osteogenic drug DEX and to enable its incorporation within the polymer matrix in the form of fibers by the electrospinning process.

Table 1. Summary of the Pore Characteristics (Pore Size, Specific Surface Area and Pore Volume) Of mBGn before and after the Amination, as Analyzed by BET Method, as well as the Surface Zeta-Potential Values

parameter	non-aminated	aminated
zeta potential (mV)	− 15.5 ± 0.61	+ 23.3 ± 1.18
S_{BET} (m^2/g)	47.2	41.5
V (cm^3/g)	0.12	0.08
pore Ø (nm)	3.54	3.51

3.2. Nanocomposite Fiber Scaffolds and Properties Favorable for Bone Grafts. The mBGn were added at varying contents (0, 2.5, 5, and 10%) to PCL-gelatin composition in order to generate fibrous scaffolds using the electrospinning technique. The SEM images of the resulting fibers (Figure 2a) clearly showed nonwoven, uniform and bead-free fibrous webs with smooth surfaces. TEM images of the scaffolds revealed the nanoparticulated form of mBGn well distributed in the polymer matrix (Figure 2b). The FT-IR spectra of the fiber scaffolds revealed characteristic bands related to mBGn (bands at 455 and 1060 cm^{-1}), which increased with increasing mBGn content (Figure 2c). TG

DOI: 10.1021/am5077759
ACS Appl. Mater. Interfaces 2015, 7, 1140−1152

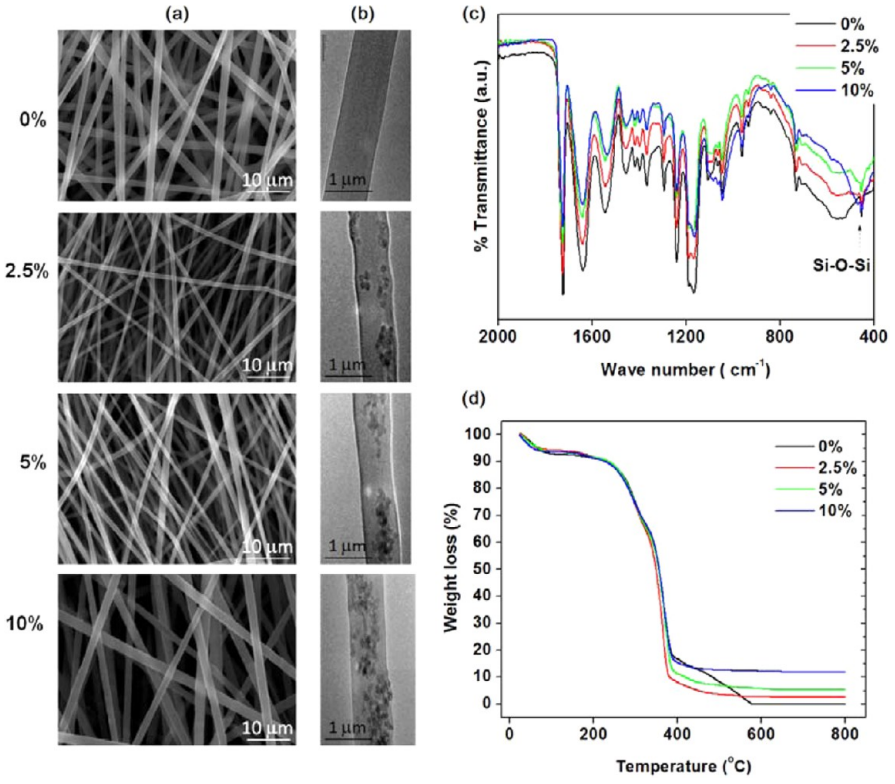

Figure 2. Characteristics of the nanocomposite fibers incorporating various contents of mBGn (0, 2.5, 5, and 10%), produced by electrospinning. Morphologies observed by (a) SEM and (b) TEM. (a) Well-developed fibrous networks were revealed for all compositions, and (b) TEM images of single fibers revealed incorporated mBGn within the fiber matrix. (c) FT-IR spectra of samples showing additional Si−O−Si band developed with mBGn incorporation. (d) TG analysis of samples showing weight loss with temperature increase, revealing the remaining weight corresponding to the quantity of mBGn initially incorporated.

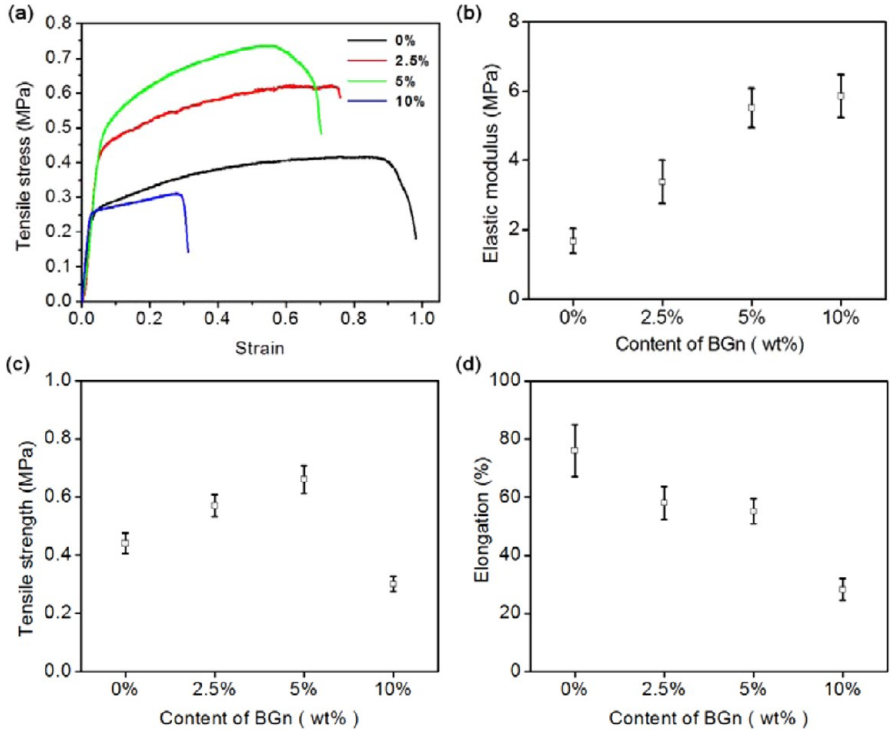

Figure 3. Tensile mechanical properties of the nanocomposite fiber scaffolds incorporating 0, 2.5, 5, and 10% mBGn. (a) Typical stress−strain curve of scaffold samples. On the basis of the stress−strain graphs, we determined (b) elastic modulus, (c) tensile strength and (d) elongation percentage. Data reported are mean ± SD and obtained from five replicate samples.

DOI: 10.1021/am5077759
ACS Appl. Mater. Interfaces 2015, 7, 1140−1152

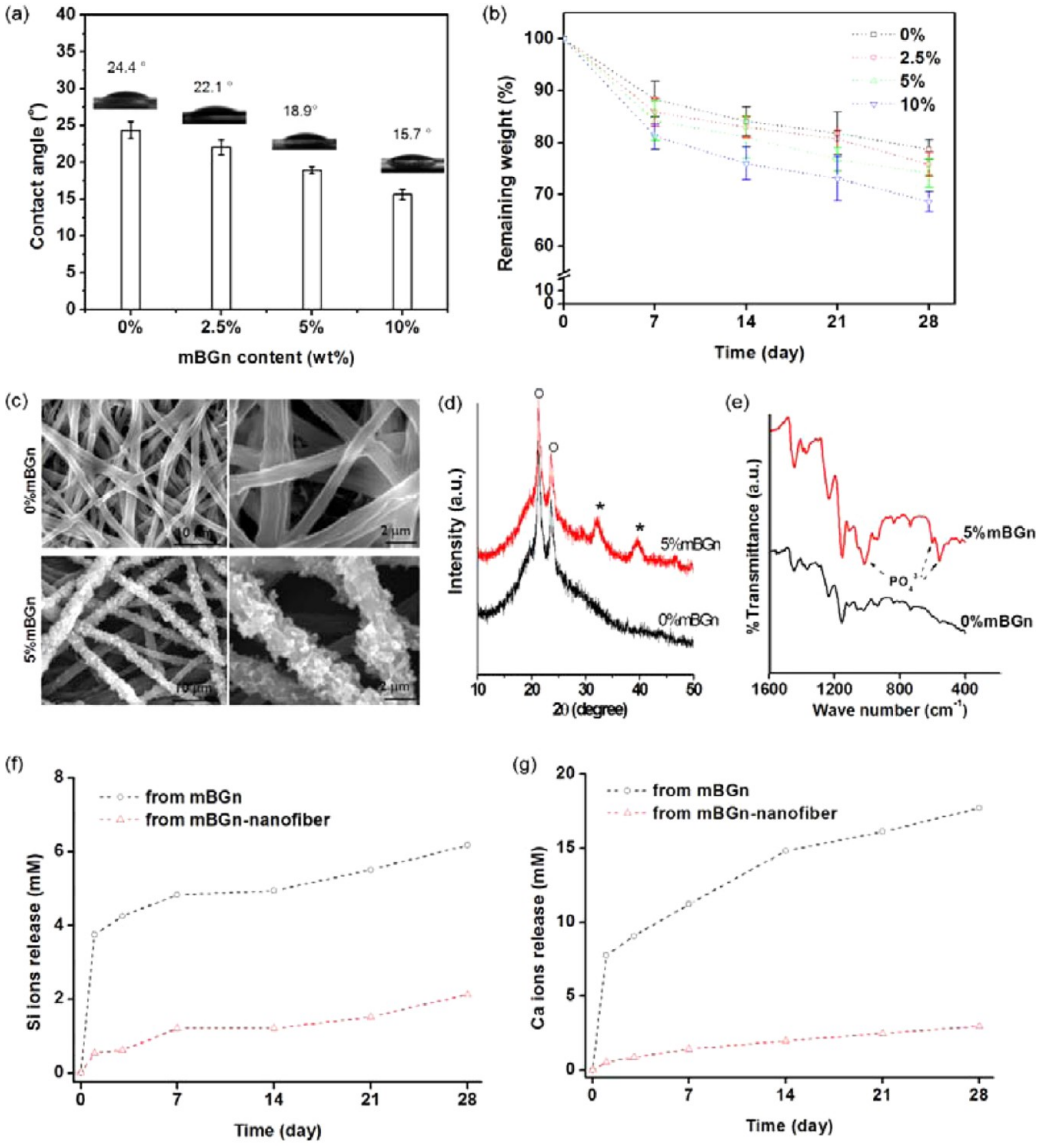

Figure 4. (a) Water contact angle of the nanocomposite fiber scaffolds incorporating mBGn (0, 2.5, 5, and 10%). Water droplet images are shown in the graph. (b) Hydrolytic degradation of fiber scaffolds with time measured in PBS for up to 28 days. (c–e) Apatite forming ability of the fiber scaffolds (0% and 5%mBGn) assessed in SBF for 28 days; (c) SEM image, (d) XRD pattern (symbol: ° PCL and * HA), and (e) FTIR analysis. (f and g) Ionic releases from the bare mBGn and the 10%mBGn fiber scaffolds; (f) Si and (g) Ca ion release profiles, quantified by ICP-AES analysis.

analysis of the scaffolds showed that the PCL-gelatin organic matrix was completely burnt out below 600 °C leaving no residues (0% remained) (Figure 2d). However, the mBGn-added scaffolds showed remnant weights after ~400 °C. The remnant weights increased with increasing mBGn content, matching the designed contents.

We next characterized the physicochemical and mechanical properties of the nanocomposite fibrous scaffolds. First, the tensile mechanical properties were measured, as shown in Figure 3. The typical stress–strain curves of different scaffolds showed a similar behavior (i.e., initial elastic region, strain <0.05), followed by a plastic deformation and then a failure (Figure 3a). Key mechanical parameters including elastic modulus, tensile strength, and elongation percentage, were calculated based on the graphs. The elastic modulus increased from 1.7 to 5.9 MPa with increasing mBGn content (Figure 3b). The tensile strength increased from 0.44 to 0.66 MPa with increasing mBGn content up to 5%, above which the strength value abruptly decreased (0.3 MPa) (Figure 3c). The elongation percentage decreased gradually from 76.1 to 28.3% with increasing mBGn content (Figure 3d). These mechanical behaviors associated with the addition of mBGn have generally been observed in the nanocomposites of flexible yet weak polymer matrix with hard nanoparticulates.[11,19] The increases in stiffness and strength accompanied by the compensation in elongation may be considered as a beneficial aspect, especially for the purpose of hard tissue regeneration.[27]

Next, the water-associated properties of the nanocomposite fiber scaffolds, including wettability, hydrolytic degradation, apatite mineral formation, and ionic releases, were examined. First, the hydrophilicity of the fiber scaffolds was characterized by a water contact angle measurement (Figure 4a). The water contact angle gradually decreased from 24.4 to 15.7° as the mBGn content increased. The charged hydrophilic nature of mBGn improved the water affinity of the scaffolds. Then, the hydrolytic degradation of the scaffolds was tested in PBS

DOI: 10.1021/am5077759
ACS Appl. Mater. Interfaces 2015, 7, 1140–1152

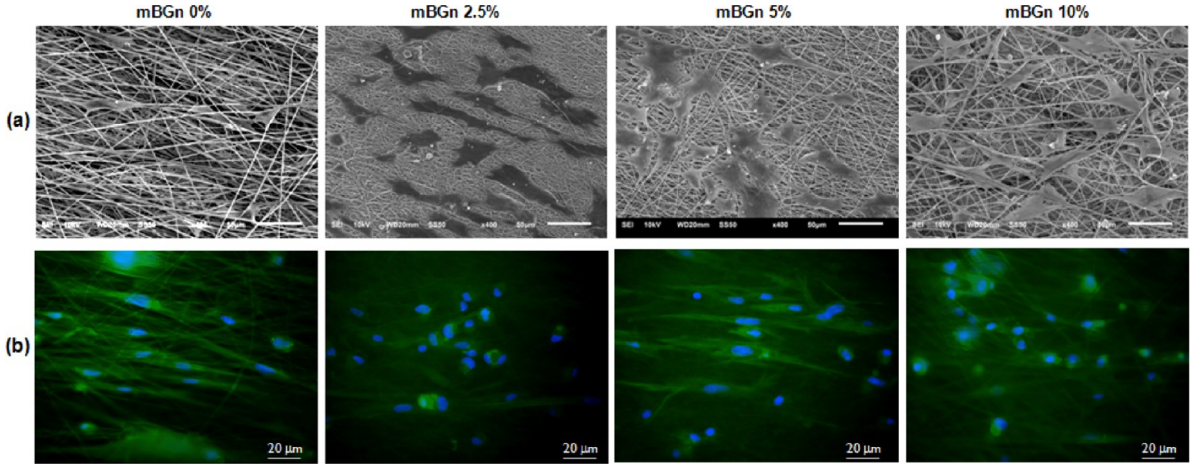

Figure 5. Cell compatibility of the fiber scaffolds generated with different compositions, briefly assessed using rat periodontal ligament stem cells (rPDSCs). After 10 days of culture on the scaffolds, (a) SEM and (b) fluorescence images of cells were observed.

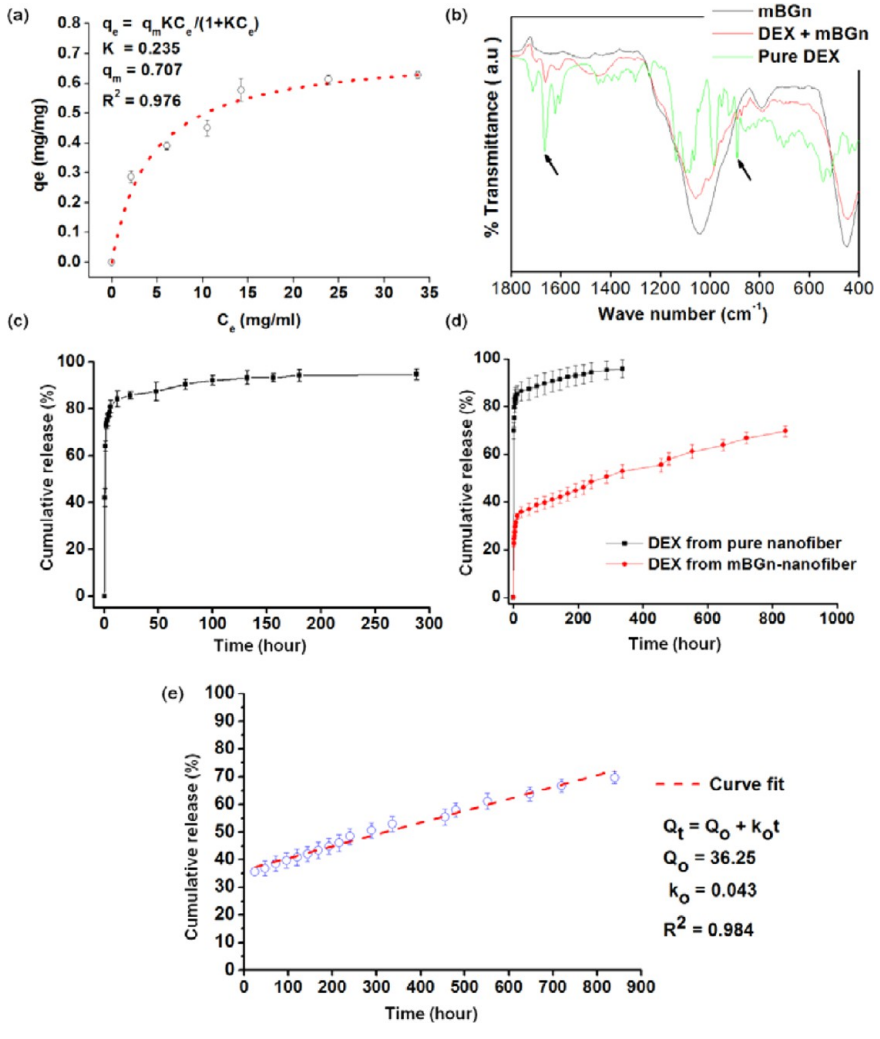

Figure 6. Drug loading and release study; (a) DEX loaded amounts onto mBGn were recorded with varying DEX concentrations at fixed mBGn content. Loading saturation was observed ~0.61 mg DEX per mg of mBGn. The DEX loading curve fitted well to Langmuir isotherm plot (parameters shown within graph). (b) FT-IR spectra of samples showing DEX loading onto mBGn. Characteristic DEX bands assigned as arrows. (c) DEX release profile from the mBGn, showing a rapid release within 24 h. (d) DEX release from the 2.5%mBGn fiber scaffolds, showing a highly sustainable release over weeks to a month after initial burst release, which was replotted in graph. (e) The DEX release data showed almost a linear behavior with a well fit to zero order kinetics model, $Q_t = 36.25 + 0.043t$ ($R^2 = 0.984$).

DOI: 10.1021/am5077759
ACS Appl. Mater. Interfaces 2015, 7, 1140−1152

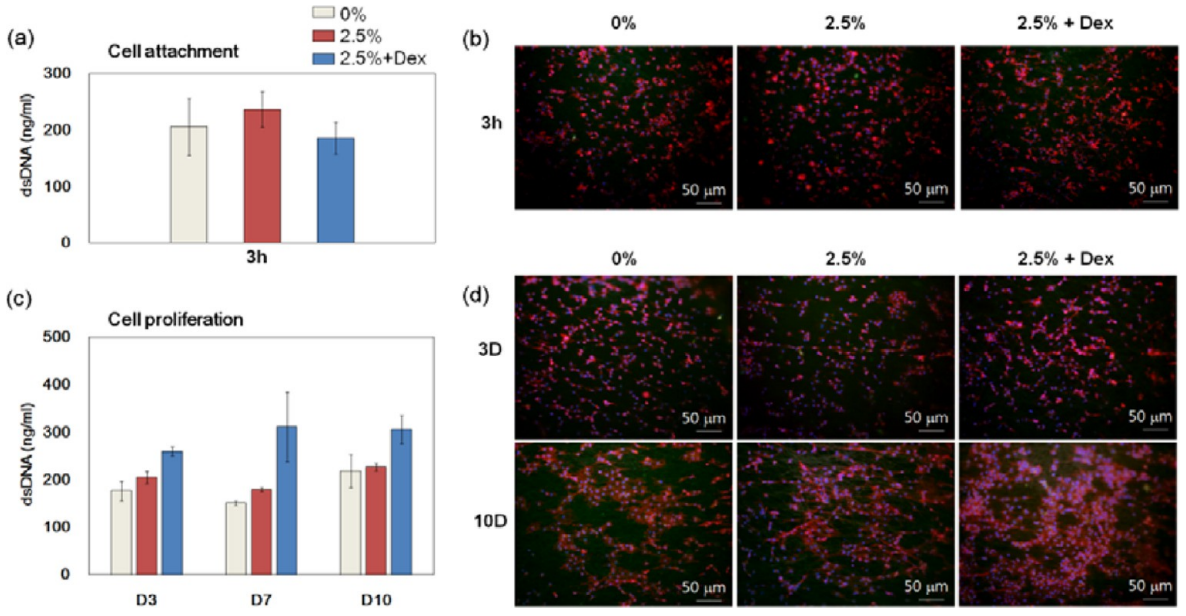

Figure 7. In vitro rPDLSCs responses to the fibrous scaffolds; (a) cell adhesion level, (b) cell adhesion morphology by CLSM, (c) cell proliferation level, and (d) cell proliferation morphology by CLSM.

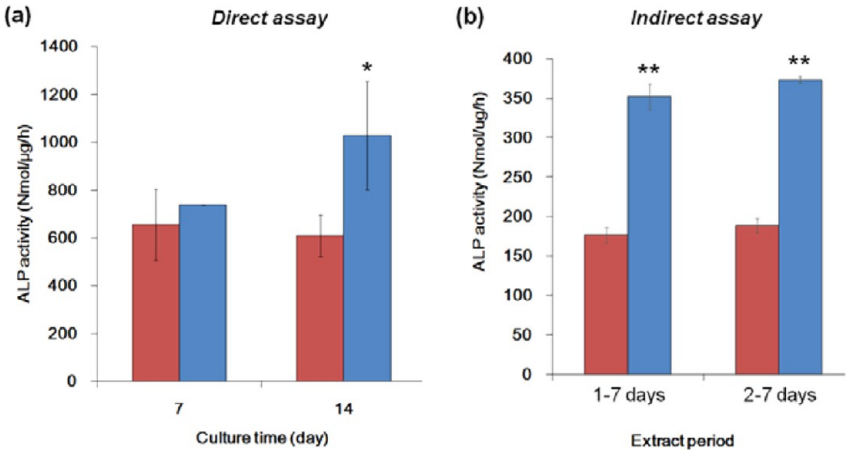

Figure 8. Effects on osteogenesis of rPDLSCs, as representatively assessed by means of ALP activity (red bars: 2.5%, blue bars: 2.5%+Dex). (a) Direct assay cultured on the scaffold sample for 7 and 14 days. (b) Indirect assay using extracts, which was carried out to confirm the therapeutic efficacy of the DEX released from the nanocomposite fiber scaffolds. Cells were seeded with the extracts prepared from the fiber scaffolds inserted in cell-free medium during the first 7 days (1−7 days) or the subsequent 7 days (2−7 days), and the ALP activity of cells was assessed after 7 days of culture. (*) $p < 0.05$, (**) $p < 0.01$ for $n = 3$, by ANOVA followed by Fisher posthoc.

solution for periods of up to 4 weeks (Figure 4b). Degradation occurred gradually with time for all the compositions, and the degradation rate increased with increasing mBGn content. As a result, after 4 weeks, the 10%mBGn scaffold degraded ∼31%, while the pure polymer scaffold degraded ∼21%. The degradation of the nanocomposites might have been enhanced by increased hydrophilicity and thus increased water attack. The apatite forming ability of the nanocomposite scaffolds in SBF was also examined. After SBF-incubation, the surface of 5% mBGn scaffold was first observed by SEM (Figure 4c). There was substantial formation of apatite nanocrystallites throughout the scaffold surface, which, however, was not readily revealed in pure polymer scaffold. The XRD pattern showed the development of apatite crystal phase in the 5%mBGn scaffold (Figure 4d), and the FT-IR spectrum also revealed the chemical bands associated with phosphate groups in apatite (Figure 4e). The results demonstrated the mBGn added to the fiber scaffolds improved the surface reactivity and acellular bone-bioactivity.

Furthermore, the release of ions (calcium and silicon) from the nanocomposite scaffolds was analyzed for periods of up to 4 weeks by ICP-AES (Figure 4f,g). The ionic release from bare mBGn, the reference group, was also recorded. The ion releases from bare mBGn were quite rapid during the first day, after which the released amounts gradually increased. As a result, about 6.2 mM of Si ions and 17.7 mM of Ca ions were released over 4 weeks. From the scaffold samples, which contained the same amount of mBGn (20 mg), the ionic releases were much less than those from the bare mBGn; about 2.1 mM of Si ions and 2.9 mM of Ca ions over 4 weeks. Of note, the initial burst effect was not observed in the scaffold, demonstrating a sustained and long-term release of both ions from the scaffold samples. The polymer matrix slows down a series of ion release processes (i.e., diffusion of water molecules to the mBGn,

DOI: 10.1021/am5077759
ACS Appl. Mater. Interfaces 2015, 7, 1140−1152

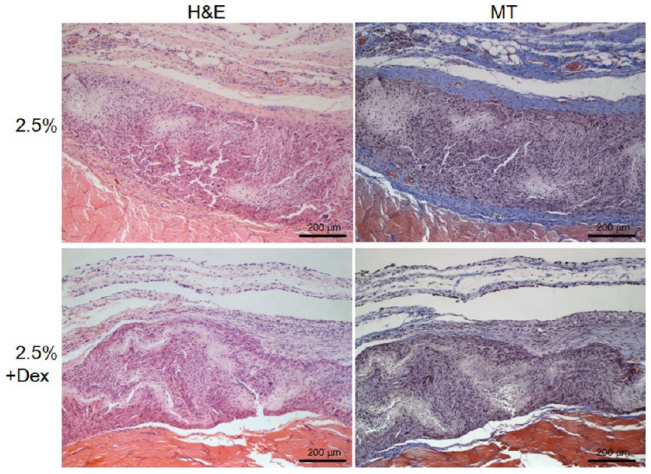

Figure 9. Tissue biocompatibility of the scaffolds incorporating 2.5% mBGn with or without DEX in rat subcutaneous model at 2 weeks postimplantation. Histological images after H&E and MT staining.

reaction between the aqueous medium and the mBGn surface, and the diffusion of ions out of the matrix). Even so, the Ca and Si ions were shown to release steadily up to 4 weeks, implying that the mBGn continued to dissolve, albeit slowly. At this point, it should be noted that the released Ca and Si ions might have some biological effects, because the concentrations of both Ca and Si ions released were at a few mM, and this concentration range has previously been suggested to significantly up-regulate several osteogenic genes.[28−32] In other words, the added mBGn can have therapeutic roles in cells for bone formation.

After assessing the physicochemical and mechanical properties of the produced nanocomposite fiber scaffolds, we briefly assessed the cell compatibility on the fibrous scaffolds with different compositions. The representative cell growth morphologies were taken by SEM and CLSM, respectively, at day 10 (Figure 5a,b). For all scaffolds, the cells were shown to grow well with highly elongated cytoskeletal processes along the fibrous substrate, reflecting the favorable cell compatibility

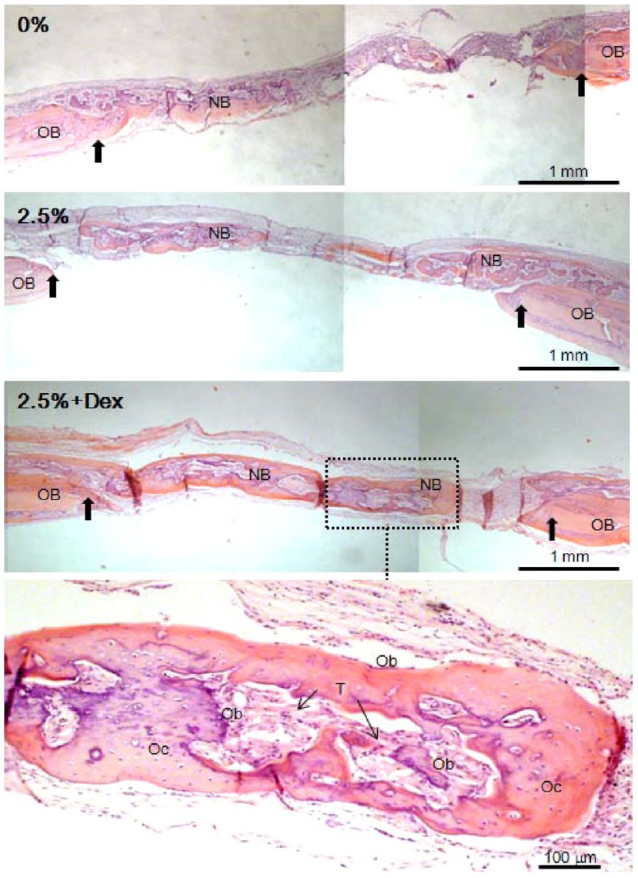

Figure 11. Histological images of samples implanted in the calvarium defect visualized after H&E staining. Dark arrows point to defect margins. Symbols are old bone (OB), new bone (NB), osteoblasts (Ob), osteocytes (Oc), and trabeculae (T). The 2.5%mBGn+DEX group was enlarged to show typical neo-bone structure.

of all compositions. On this basis, further assays on the biological efficacy of the scaffolds were designed in detail, targeting the effects of DEX delivery.

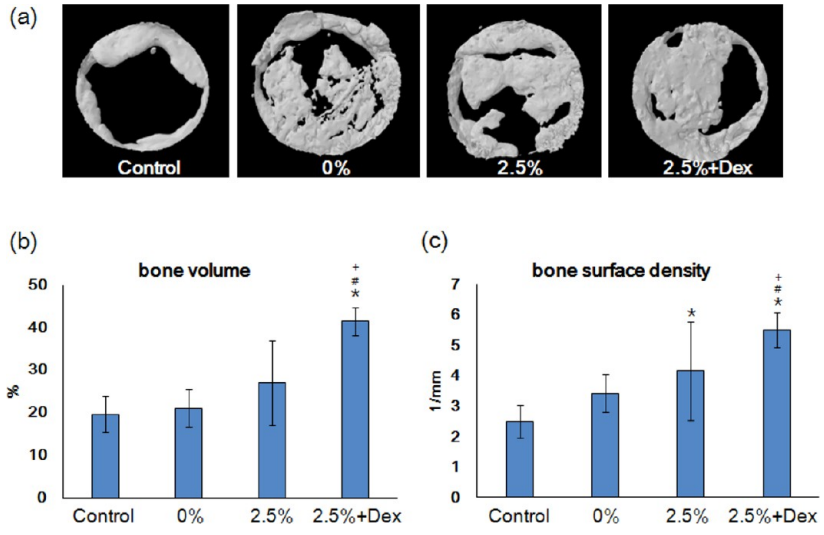

Figure 10. In vivo bone regeneration ability of the DEX-releasing therapeutic fiber scaffolds, as assessed in rat calvarium model. After 6 week implantation, (a) micro-CT images were obtained, and the (b) bone volume and (c) bone surface density were analyzed. (*) $p < 0.05$ vs control, (#) $p < 0.05$ vs 0%, (+) $p < 0.05$ vs 2.5%, for $n = 3$, by ANOVA followed by Fisher posthoc.

DOI: 10.1021/am5077759
ACS Appl. Mater. Interfaces 2015, 7, 1140−1152

3.3. Effective Loading of DEX and Long-Term Release Profiles. The loading capacity of DEX molecules within the mBGn nanocarriers was first examined. The DEX quantity loaded onto mBGn was measured with varying DEX concentration, using UV−vis spectroscopy. Figure 6a shows the loading isotherm of DEX onto mBGn. The DEX loading quantity increased gradually from 0.286 to 0.627 mg (per mg mBGn) when DEX concentration used was varied from 5 to 15 mg/mL, after which the DEX loading appeared to plateau. The obtained loading isotherm was fitted to a modified Langmuir isotherm model, according to the following equation: $q_e = q_m KC_e/(1 + KC_e)$,[33] where q_m is the maximum loaded amount (mg/mg), C_e is the equilibrium concentration, and K is a kinetic constant. The experimental data fit quite well to the Langmuir model with $R^2 = 0.976$, $K = 0.235$, and $q_m = 0.707$ (also shown within the graph). The FT-IR spectra of samples showed characteristic bands of DEX at about 890 and 1668 cm^{-1} in the DEX-loaded mBGn (Figure 6b).

Next, the in vitro release of DEX from mBGn was recorded by UV−vis spectroscopy (Figure 6c). The DEX release was very abrupt initially, with almost 80% being released within 24 h. On the other hand, when the DEX-loaded mBGn was incorporated (at 2.5%) within the fiber scaffold, the DEX release test was carried out using HPLC. DEX release from fiber matrix was also included for comparison purpose. The DEX release from the nanocomposite fiber scaffold showed an initial rapid release within 1 day followed by a sustainable release up to 28 days (Figure 6d). The initial burst release of DEX was ∼35% within 24 h, and after this, the DEX release was very sustainable with an almost linear pattern leading to ∼35% DEX release over as long as ∼5 weeks. The postburst DEX release data was analyzed using a zero order kinetics equation,[34] $Q_t = Q_o + k_o t$, where Q_t is the amount of drug released at time t, Q_o is the initial amount of drug released (a result of initial burst), and k_o the is a zero-order release constant. The DEX release data were well fitted to the linear equation with $R^2 = 0.984$ (Figure 6e). The kinetic constants are summarized within the graphs. The initial rapid release of DEX at the very beginning of the release test reflects the burst effect of drug molecules loosely adhered to the surface of the fiber scaffolds either from the surface-exposed mBGn or originating from some DEX molecules prereleased in the biopolymer matrix during the mixing step. However, soon after the burst effect within 24 h, the zero-order kinetic behavior of DEX release was very intriguing, which signifies a promising aspect of the scaffold as the ideal drug delivery system.[35−37] The ease of dissociation of DEX from the mBGn and the excellent hydrophilicity and degradation of the fiber matrix are deemed to result in the linear release of DEX, which does not follow the parabolic pattern or power law. On the basis of the DEX release study, it was evident that the approach of DEX-preloading within the mBGn in concert with its incorporation within the hydrophilic biopolymeric matrix was highly effective in achieving a long-term zero-order DEX release, a pattern that is considered to potentiate the biological effects of loaded drugs.

3.4. In Vitro Effects on Cell Proliferation and Osteogenesis. After confirming the effective loading of DEX molecules within the engineered fiber scaffolds and their subsequent long-term release behaviors, we next sought to identify the biological functions elicited using relevant tissue cells. For this, stem cells derived from periodontal ligament of rat (rPDLSCs) were used. Fibrous scaffolds with a membrane-like form are thought to be efficient for guided bone regeneration and reconstruction of periodontal pockets, where the rPDLSCs play critical roles in the formation of bone as well as periodontal ligament.[38−40] We used three representative sample groups for the tests; mBGn-absent scaffold (0%), 2.5%mBGn-added scaffold (2.5%), and 2.5% mBGn with DEX-loaded scaffold (2.5%+DEX). The use of 2.5%mBGn was based on the DEX release study. The addition of only 2.5%mBGn to the scaffold was considered to release DEX molecules with doses effective for the cellular responses. First, the in vitro cell responses to the scaffolds were assessed in terms of cell adhesion and proliferation. On all the scaffolds, the cells initially adhered actively (for 3 h), as revealed by the dsDNA quantity of cells (Figure 7a) and nuclei-stained cell images (Figure 7b). Additionally, the cells cultured for up to 10 days were shown to have extended cytoskeletal processes along the underlying fibrous structure (Figure 7c,d). There were few differences between the scaffold groups in the cell adhesion and proliferation stages.

While DEX had no significant effects on the proliferative capacity of the rPDLSCs, the osteogenic differentiation behavior of cells was substantially influenced. As an index of osteogenesis, the alkaline phosphatase (ALP) activity of cells was determined comparing the representative two groups (2.5% and 2.5%+DEX). First, the cells cultured for 7 and 14 days were assayed for ALP quantification. Cells cultured on 2.5%mBGn+DEX sample had significantly higher ALP activity particularly at 14 days (Figure 8a). The results appeared to indicate the possibility of the effect of DEX released from the scaffolds on the ALP stimulation. We further sought to elucidate whether the effect was indeed from the released DEX, and for this, we collected extracts from the fiber scaffolds and used the extracts as the culture medium. Extracts were collected over two periods: the initial 7 days (1−7 days) and the following 7 days (2−7 days), which were then cultured with cells over 7 days and the ALP activity was analyzed (Figure 8b). Significantly higher levels of ALP were produced by the cells for both of the first and second periods of extracts. It is noteworthy that the ALP stimulation was similar at both periods, suggesting that the effects of DEX released in the different periods were quite uniform with time and thus the long-term stimulating potential of the DEX release.

In fact, some recent studies have engineered bone scaffolds to deliver DEX more effectively and controllably. Yang et al. have developed poly(lactic-*co*-glycolic acid) (PLGA)/tricalcium phosphate composite scaffolds to show the possible controllable release of DEX and protein bovine serum albumin.[41] Furthermore, Su et al. utilized the core−shell structured poly(l-lactic acid)-collagen fiber for the delivery of DEX with bone morphogenetic protein 2, and showed the delivered DEX molecules stimulated the ALP activity of MSCs.[42] For the inflammation control and angiogenesis, the DEX drug was also used in combination with vascular endothelial growth factor within the PLGA microspheres/poly(vinyl alcohol) hydrogel composites.[35] In the present study, we designed a fiber scaffold system incorporating novel bone-bioactive mesoporous nanospheres that could carry DEX drug, and demonstrated its long-term delivery and the effective roles in stimulating osteogenesis of stem cells. Next, we sought to confirm the in vivo feasibility of the developed DEX-releasing scaffolds in defective bone tissues.

3.5. Efficacy under in Vivo Bone Regeneration Model. First, for the examination of in vivo safety of the DEX releasing

DOI: 10.1021/am5077759
ACS Appl. Mater. Interfaces 2015, 7, 1140−1152

fiber scaffolds, we implanted scaffolds in rat subcutaneous tissues. After the implantation of the DEX-free and DEX-loaded nanocomposite scaffolds for 2 weeks, the histological examinations by H&E and MT stains showed that both implanted scaffolds were biocompatible at 2 weeks with many fibroblastic cells found within the scaffold area, as shown in Figure 9. Thin fibrous capsules with neovascularization were also observed around the samples. The status of cells and tissues in the surrounding or penetrated area within both scaffolds indicates no tissue rejection through the implantation period, with very minimal inflammatory reactions related with the scaffolds. These biological responses are generally found in biocompatible materials[10,11,43] and are indicative of the sound tissue responses to the engineered scaffolds.

On the basis of this observation, we next investigated the bone regeneration ability of the scaffolds in a rat calvarium defect model. Sample groups were implanted for 6 weeks in 5 mm critical-sized calvarium; then, the samples were harvested, and the new bone formation was analyzed using μCT and histological staining. All animals showed a good healing response without adverse tissue reactions. During sacrifice, the implanted areas were stable, and any visible fibrous invasions or signs of internal inflammation were not detected on harvested tissues.

The reconstructed 3D images of the samples showed calcified tissues formed within the defect regions (Figure 10a). The newly formed bone was further analyzed in terms of bone quantity (bone volume, Figure 10b) and quality (bone surface density, Figure 10c). Compared to blank control or pure fiber scaffold group, the nanocomposite scaffold group showed some increase in the bone volume and density, although the difference was not so significant. Furthermore, the DEX-loaded nanocomposite group showed significantly higher levels of bone volume and bone surface density. Results showed the effective role of the DEX release in the new bone formation around the fiber scaffolds.

We further examined histological microscopic findings of H&E stained samples, as presented in Figure 11. New bone tissue generally grows from the defect margins toward the central zone; therefore, some limited bone ingrowth was noticed in the control and pure scaffold groups; however, in the 2.5%+DEX group, there was substantial neo-bone formation, which appeared to begin at the caudal edge of the defect area covered by the scaffold and then grow massively into the scaffold central part. On closer examination, a number of osteoblasts (Ob) lining the neo-bone tissues and osteocytes (Oc) embedded within were revealed. Active cellular processes within the trabeculae (T) further indicated the regenerative processes of matrix deposition and calcification. The bone structure also demonstrated the state of immature woven bone, which can become mature lamellar bone with time, possibly followed by the remodeling process,[44−47] which may be manifested by implantation for longer periods. On the basis of the in vivo findings in calvarium defect, the DEX release from the nanocomposite fibrous scaffolds was proven to stimulate the bone forming processes, in terms of the quantity and quality of neo-bone structure, and the system is thus considered as a promising osteogenic stimulating platform for bone repair and regeneration.

4. CONCLUSIONS

Novel nanocomposite fibrous scaffolds were proposed for the purpose of bone regeneration, and the effects of osteogenic drug delivery on in vitro stem cell responses and in vivo bone formation were demonstrated. Mesoporous nanocarriers incorporated within biopolymer fiber matrix were shown to load DEX molecules effectively and deliver them in a highly sustained manner for more than 1 month. Through the DEX delivery, the stem cells derived from periodontal ligament were highly stimulated to an osteogenic lineage, and in vivo bone formation in the calvarium model was significantly improved. The currently exploited drug delivering scaffolds are considered to be a potential osteogenic stimulating platform for bone regeneration.

AUTHOR INFORMATION

Corresponding Author

*Tel: +82 41 550 3081. Fax: +82 41 550 3085. E-mail: kimhw@dku.edu.

Notes

The authors declare no competing financial interest.

ACKNOWLEDGMENTS

This work was supported by the National Research Foundation of Korea, Republic of Korea (Priority Research Centers Program; No. 2009-0093829 and No. NRF-2013R1A1A2013414). The authors would like to thank Kim HS for her help in HPLC assays.

REFERENCES

(1) Kent, L. J.; Kaigler, D.; Wang, Z.; Krebsbach, P. H.; Mooney, D. J. Coating of VEGF-Releasing Scaffolds with Bioactive Glass for Angiogenesis and Bone Regeneration. *Biomaterials* **2006**, *27*, 3249−3255.

(2) Hong, K. S.; Kim, E. C.; Bang, S. H.; Chung, C. H.; Lee, Y. I.; Hyun, J. K.; Lee, H. H.; Jang, J. H.; Kim, H. W. Bone Regeneration by Bioactive Hybrid Membrane Containing FGF2 within Rat Calvarium. *J. Biomed. Mater. Res., Part A* **2010**, *94*, 1187−1194.

(3) Lee, J. H.; Park, J. H.; El-Fiqi, A.; Kim, J. H.; Yun, Y. R.; Jang, J. H.; Han, C. M.; Lee, E. J.; Kim, H. W. Biointerface Control of Electrospun Fiber Scaffolds for Bone Regeneration: Engineered Protein Link to Mineralized Surface. *Acta Biomater.* **2014**, *10*, 2750−2761.

(4) Kim, H. W.; Kim, H. E.; Salih, V. Stimulation of Osteoblast Responses to Biomimetic Nanocomposites of Gelatin-Hydroxyapatite for Tissue Engineering Scaffolds. *Biomaterials* **2005**, *26*, 5221−30.

(5) Gao, C.; Gao, Q.; Li, Y.; Rahaman, M. N.; Teramoto, A.; Abe, K. In Vitro Evaluation of Electrospun Gelatin-Bioactive Glass Hybrid Scaffolds for Bone Regeneration. *J. Appl. Poly. Sci.* **2013**, *127*, 2588−2599.

(6) Gandhimathi, C.; Venugopal, J.; Ravichandran, R.; Sundarrajan, S.; Suganya, S.; Ramakrishna, S. Mimicking Nanofibrous Hybrid Bone Substitute for Mesenchymal Stem Cells Differentiation into Osteogenesis. *Macromol. Biosci.* **2013**, *13*, 696−706.

(7) Shin, S. H.; Purevdorj, O.; Castano, O.; Planell, J. A.; Kim, H. W. A Short Review: Recent Advances in Electrospinning for Bone Tissue Regeneration. *J. Tissue Eng.* **2012**, *3*, 2041731412443530.

(8) Ravichandran, R.; Venugopal, J. R.; Sundarrajan, S.; Mukherjee, S.; Ramakrishna, S. Precipitation of Nanohydroxyapatite on PLLA/PBLG/Collagen Nanofibrous Structures for the Differentiation of Adipose Derived Stem Cells to Osteogenic Lineage. *Biomaterials* **2012**, *33*, 846−55.

(9) El-Fiqi, A.; Kim, H.-W. Mesoporous Bioactive Nanocarriers in Electrospun Biopolymer Fibrous Scaffolds Designed for Sequential Drug Delivery. *RSC Advances* **2014**, *4*, 4444−4452.

(10) Castano, O.; Sachot, N.; Xuriguera, E.; Engel, E.; Planell, J. A.; Park, J. H.; Jin, G. Z.; Kim, T. H.; Kim, J. H.; Kim, H. W. Angiogenesis in Bone Regeneration: Tailored Calcium Release in Hybrid Fibrous Scaffolds. *ACS Appl. Mater. Interfaces* **2014**, *6*, 7512−22.

DOI: 10.1021/am5077759
ACS Appl. Mater. Interfaces 2015, 7, 1140−1152

(11) Singh, R. K.; Patel, K. D.; Lee, J. H.; Lee, E. J.; Kim, J. H.; Kim, T. H.; Kim, H. W. Potential of Magnetic Nanofiber Scaffolds with Mechanical and Biological Properties Applicable for Bone Regeneration. *PLoS One* **2014**, *9*, e91584.
(12) Jegal, S. H.; Park, J. H.; Kim, J. H.; Kim, T. H.; Shin, U. S.; Kim, T. I.; Kim, H. W. Functional Composite Nanofibers of Poly(lactide-co-caprolactone) Containing Gelatin-Apatite Bone Mimetic Precipitate for Bone Regeneration. *Acta Biomater.* **2011**, *7*, 1609−17.
(13) Hanemann, T.; Szabó, D. V. Polymer−Nanoparticle Composites: From Synthesis to Modern Applications. *Materials* **2010**, *3*, 3468−3517.
(14) Hodgkinson, T.; Yuan, X. F.; Bayat, A. Electrospun Silk Fibroin Fiber Diameter Influences in Vitro Dermal Fibroblast Behavior and Promotes Healing of ex Vivo Wound Models. *J. Tissue Eng.* **2014**, *5*, 2041731414551763.
(15) Lee, H. H.; Yu, H. S.; Jang, J. H.; Kim, H. W. Bioactivity Improvement of Poly(ε-caprolactone) Membrane with the Addition of Nanofibrous Bioactive Glass. *Acta Biomater.* **2008**, *4*, 622−629.
(16) Kouhi, M.; Morshed, M.; Varshosaz, J.; Fathi, M. H. Poly(ε-caprolactone) Incorporated Bioactive Glass Nanoparticles and Simvastatin Nanocomposite Nanofibers: Preparation, Characterization and in Vitro Drug Release for Bone Regeneration Applications. *Chem. Eng. J.* **2013**, *228*, 1057−1065.
(17) Wutticharoenmongkol, P.; Sanchavanakit, N.; Pavasant, P.; Supaphol, P. Preparation and Characterization of Novel Bone Scaffolds Based on Electrospun Polycaprolactone Fibers Filled with Nanoparticles. *Macromol. Biosci.* **2006**, *6*, 70−77.
(18) Song, B.; Wu, C.; Chang, J. Dual Drug Release from Electrospun Poly(lactic-co-glycolic acid)/Mesoporous Silica Nanoparticles Composite Mats with Distinct Release Profiles. *Acta Biomater.* **2012**, *8*, 1901−7.
(19) Qiu, K.; He, C.; Feng, W.; Wang, W.; Zhou, X.; Yin, Z.; Chen, L.; Wang, H.; Mo, X. Doxorubicin-Loaded Electrospun Poly(l-lactic acid)/Mesoporous Silica Nanoparticles Composite Nanofibers for Potential Postsurgical Cancer Treatment. *J. Mater. Chem. B* **2013**, *1*, 4601−4611.
(20) Hou, Z.; Li, X.; Li, C.; Dai, Y.; Ma, P. a.; Zhang, X.; Kang, X.; Cheng, Z.; Lin, J. Electrospun Upconversion Composite Fibers as Dual Drugs Delivery System with Individual Release Properties. *Langmuir* **2013**, *29*, 9473−9482.
(21) Kwon, S.; Sing, R.; Perez, R.; Abou Neel, E. A.; Kim, H. W.; Chrzanowski, W. Silica-Based Mesoporous Nanoparticles for Controlled Drug Delivery. *J. Tissue Eng.* **2013**, *4*, 2041731413503357.
(22) Kim, T. H.; Eltohamy, M.; Kim, M.; Perez, R.; Kim, J. H.; Yun, Y. R.; Jang, J. H.; Lee, E. J.; Knowles, J. C.; Kim, H. W. Therapeutic Foam Scaffolds Incorporating Biopolymer-Shelled Mesoporous Nanospheres with Growth Factors. *Acta Biomater.* **2014**, *10*, 2612−2621.
(23) Kwon, S.; Singh, R.; Kim, T. H.; Patel, K.; Kim, J. J.; Chrzanowski, W.; Kim, H. W. Luminescent Mesoporous Nanoreservoirs for the Effective Loading and Intracellular Delivery of Therapeutic Drugs. *Acta Biomater.* **2014**, *10*, 1431−1442.
(24) El-Fiqi, A.; Kim, T. H.; Kim, M.; Eltohamy, M.; Won, J. E.; Lee, E. J.; Kim, H. W. Capacity of Mesoporous Bioactive Glass Nanoparticles to Deliver Therapeutic Molecules. *Nanoscale* **2012**, *4*, 7475−88.
(25) El-Fiqi, A.; Lee, J. H.; Lee, E. J.; Kim, H. W. Collagen Hydrogels Incorporated with Surface-Aminated Mesoporous Nanobioactive Glass: Improvement of Physicochemical Stability and Mechanical Properties is Effective for Hard Tissue Engineering. *Acta Biomater.* **2013**, *9*, 9508−9521.
(26) Park, J. H.; Kim, M. K.; El-Fiqi, A.; Seo, S. J.; Lee, E. J.; Kim, J. H.; Kim, H. W. Bioactive and Porous-Structured Nanocomposite Microspheres Effective for Cell Delivery: A Feasibility Study for Bone Tissue Engineering. *RSC Adv.* **2014**, *4*, 29062−29071.
(27) Roel, G. M.; Breuls, T.; Jiya, U.; Smit, T. H. Scaffold Stiffness Influences Cell Behavior: Opportunities for Skeletal Tissue Engineering. *Open Orthop. J.* **2008**, *2*, 103−109.
(28) Hench, L. L. Genetic Design of Bioactive Glass. *J. Eur. Ceram. Soc.* **2009**, *29*, 1257−1265.
(29) Maeno, S.; Niki, Y.; Matsumoto, H.; Morioka, H.; Yatabe, T.; Funayama, A.; Toyama, Y.; Taguchi, T.; Tanaka, J. The Effect of Calcium Ion Concentration on Osteoblast Viability, Proliferation and Differentiation in Monolayer and 3D Culture. *Biomaterials* **2005**, *26*, 4847−55.
(30) Saffarian Tousi, N.; Velten, M. F.; Bishop, T. J.; Leong, K. K.; Barkhordar, N. S.; Marshall, G. W.; Loomer, P. M.; Aswath, P. B.; Varanasi, V. G. Combinatorial Effect of Si^{4+}, Ca^{2+}, and Mg^{2+} Released from Bioactive Glasses on Osteoblast Osteocalcin Expression and Biomineralization. *Mater. Sci. Eng., C* **2013**, *33*, 2757−2765.
(31) Zhai, W.; Lu, H.; Wu, C.; Chen, L.; Lin, X.; Naoki, K.; Chen, G.; Chang, J. Stimulatory Effects of the Ionic Products from Ca−Mg−Si Bioceramics on both Osteogenesis and Angiogenesis in Vitro. *Acta Biomater.* **2013**, *9*, 8004−8014.
(32) Varanasi, V. G.; Saiz, E.; Loomer, P. M.; Ancheta, B.; Uritani, N.; Ho, S. P.; Tomsia, A. P.; Marshall, S. J.; Marshall, G. W. Enhanced Osteocalcin Expression by Osteoblast-Like Cells (MC3T3-E1) Exposed to Bioactive Coating Glass (SiO_2−CaO−P_2O_5−MgO−K_2O−Na_2O System) Ions. *Acta Biomater.* **2009**, *5*, 3536−3547.
(33) Smirnova, I.; Mamic, J.; Arlt, W. Adsorption of Drugs on Silica Aerogels. *Langmuir* **2003**, *19*, 8521−8525.
(34) Hughes, G. A. Nanostructure-Mediated Drug Delivery. *Nanomedicine* **2005**, *1*, 22−30.
(35) Patil, S. D.; Papadmitrakopoulos, F.; Burgess, D. J. Concurrent Delivery of Dexamethasone and VEGF for Localized Inflammation Control and Angiogenesis. *J. Controlled Release* **2007**, *117*, 68−79.
(36) Wang, Q.; Wang, J.; Lu, Q.; Detamore, M. S.; Berkland, C. Injectable PLGA Based Colloidal Gels for Zero-Order Dexamethasone Release in Cranial Defects. *Biomaterials* **2010**, *31*, 4980−6.
(37) Jayant, R. D.; McShane, M. J.; Srivastava, R. Polyelectrolyte-Coated Alginate Microspheres as Drug Delivery Carriers for Dexamethasone Release. *Drug Delivery* **2009**, *16*, 331−40.
(38) Moshaverinia, A.; Chen, C.; Xu, X.; Akiyama, K.; Ansari, S.; Zadeh, H. H.; Shi, S. Bone Regeneration Potential of Stem Cells Derived from Periodontal Ligament or Gingival Tissue Sources Encapsulated in RGD-Modified Alginate Scaffold. *Tissue Eng., Part A* **2014**, *20*, 611−21.
(39) Moshaverinia, A.; Chen, C.; Akiyama, K.; Xu, X.; Chee, W. W.; Schricker, S. R.; Shi, S. Encapsulated Dental-Derived Mesenchymal Stem Cells in an Injectable and Biodegradable Scaffold for Applications in Bone Tissue Engineering. *J. Biomed. Mater. Res., Part A* **2013**, *101*, 3285−94.
(40) Kim, J. H.; Park, C. H.; Perez, R.; Lee, H. Y.; Jang, J. H.; Lee, H. H.; Wall, I. B.; Shi, S.; Kim, H. W. Advanced Biomatrix Designs for Regenerative Therapy of Periodontal Tissues. *J. Dent. Res.* **2014**, *93*, 1203−1211.
(41) Yang, Y.; Tang, G.; Zhang, H.; Zhao, Y.; Yuan, X.; Wang, M.; Yuan, X. Controllable Dual-Release of Dexamethasone and Bovine Serum Albumin from PLGA/Beta-Tricalcium Phosphate Composite Scaffolds. *J. Biomed. Mater. Res., Part B* **2011**, *96*, 139−51.
(42) Su, Y.; Su, Q.; Liu, W.; Lim, M.; Venugopal, J. R.; Mo, X.; Ramakrishna, S.; Al-Deyab, S. S.; El-Newehy, M. Controlled Release of Bone Morphogenetic Protein 2 and Dexamethasone Loaded in Core-Shell PLLACL-Collagen Fibers for Use in Bone Tissue Engineering. *Acta Biomater.* **2012**, *8*, 763−71.
(43) Kim, J. H.; Moon, H. J.; Kim, T. H.; Jo, J. M.; Yang, S. H.; Naskar, D.; Kundu, S. C.; Chrzanowski, W.; Kim, H. W. A Novel in Vivo Platform for Studying Alveolar Bone Regeneration in Rat. *J. Tissue Eng.* **2013**, *3*, 2041731413517705.
(44) Kini, U.; Nandeesh, B. N., Physiology of Bone Formation, Remodeling, and Metabolism. In *Radionuclide and Hybrid Bone Imaging*, Fogelman, I.; Gnanasegaran, G.; van der Wall, H., Eds. Springer: Berlin, 2012; Chapter 2, pp 29−57.
(45) Foo, T.; Reagan, J.; Watson, J. T.; Moed, B. R.; Zhang, Z. External Fixation of Femoral Defects in Athymic Rats: Applications for Human Stem Cell Implantation and Bone Regeneration. *J. Tissue Eng.* **2013**, *3*, 2041731413486368.

DOI: 10.1021/am5077759
ACS Appl. Mater. Interfaces 2015, 7, 1140−1152

(46) Raggatt, L. J.; Partridge, N. C. Cellular and Molecular Mechanisms of Bone Remodeling. *J. Biol. Chem.* **2010**, *285*, 25103−25108.
(47) Sims, N. A.; Gooi, J. H. Bone Remodeling: Multiple Cellular Interactions Required for Coupling of Bone Formation and Resorption. *Semin. Cell Dev. Biol.* **2008**, *19*, 444−451.

DOI: 10.1021/am5077759
ACS Appl. Mater. Interfaces 2015, 7, 1140−1152